ISSN 1674-1056

中国物理B
Chinese Physics B

Volume 22 Number 9 September 2013

Formerly *Chinese Physics*

A Series Journal of the Chinese Physical Society
Distributed by IOP Publishing

Online: iopscience.iop.org/cpb
cpb.iphy.ac.cn

CHINESE PHYSICAL SOCIETY
IOP Publishing

Chinese Physics B (First published in 1992)

Published monthly in hard copy by the Chinese Physical Society and online by IOP Publishing, Temple Circus, Temple Way, Bristol BS1 6HG, UK

Institutional subscription information: 2013 volume

For all countries, except the United States, Canada and Central and South America, the subscription rate is £977 per annual volume.

Single-issue price £97. Delivery is by air-speeded mail from the United Kingdom.

Orders to:

Journals Subscription Fulfilment, IOP Publishing, Temple Circus, Temple Way, Bristol BS1 6HG, UK

For the United States, Canada and Central and South America, the subscription rate is US$1930 per annual volume. Single-issue price US$194. Delivery is by transatlantic airfreight and onward mailing.

Orders to:

IOP Publishing, PO Box 320, Congers, NY 10920-0320, USA

Supported by the National Natural Science Foundation of China, the China Association for Science and Technology, and the Science Publication Foundation, Chinese Academy of Sciences

Editorial Office: Institute of Physics, Chinese Academy of Sciences, PO Box 603, Beijing 100190, China

Tel: (86 – 10) 82649026 or 82649519, Fax: (86 – 10) 82649027, E-mail: cpb@aphy.iphy.ac.cn

主管单位: 中国科学院
主办单位: 中国物理学会和中国科学院物理研究所
承办单位: 中国科学院物理研究所
主　　编：欧阳钟灿
出　　版：中国物理学会
印刷装订：北京科信印刷厂
编　　辑: Chinese Physics B 编辑部
国内发行: Chinese Physics B 出版发行部
国外发行: IOP Publishing Ltd
发行范围: 公开发行
国际统一刊号: ISSN 1674–1056

国内统一刊号: CN 11–5639/O4
广告经营许可证：京海工商广字第0335号
编辑部地址: 北京 中关村 中国科学院物理研究所内
通 讯 地 址: 100190 北京 603 信箱
Chinese Physics B 编辑部
电　　话: (010) 82649026, 82649519
传　　真: (010) 82649027
E-mail: cpb@aphy.iphy.ac.cn
"Chinese Physics B"网址:
http://cpb.iphy.ac.cn(编辑部)
http://iopscience.iop.org/cpb (IOP)

Published by the Chinese Physical Society

(*Continued*)

TOPICAL REVIEW — Low-dimensional nanostructures and devices

Unique electrical properties of nanostructured diamond cones*

Gu Chang-Zhi(顾长志)[a)†], Wang Qiang(王 强)[b)], Li Jun-Jie(李俊杰)[a)‡], and Xia Ke(夏 钶)[c)]

[a)] *Beijing National Laboratory for Condensed Matter Physics, Institute of Physics, Chinese Academy of Sciences, Beijing* 100190, *China*
[b)] *Department of Applied Physics, Harbin Institute of Technology at Weihai, Weihai* 264209, *China*
[c)] *Department of Physics, Beijing Normal University, Beijing* 100875, *China*

(Received 2 August 2013)

The preparation and electrical properties of diamond nanocones are reviewed, including a maskless etching process and mechanism of large-area diamond conical nanostructure arrays using a hot filament chemical vapor deposition (HFCVD) system with negatively biased substrates, and the field electron emission, gas sensing, and quantum transport properties of a diamond nanocone array or an individual diamond nanocone. Optimal cone aspect ratio and array density are investigated, along with the relationships between the cone morphologies and experimental parameters, such as the CH_4/H_2 ratio of the etching gas, the bias current, and the gas pressure. The reviewed experiments demonstrate the possibility of using nanostructured diamond cones as a display device element, a point electron emission source, a gas sensor or a quantum device.

Keywords: diamond, nanocone, quantum device

PACS: 81.05.ug, 81.07.–b, 73.63.Rt **DOI:** 10.1088/1674-1056/22/9/098107

1. Introduction

Low-dimensional nanostructured materials such as nanopillars, nanowires, nanocones, etc., especially those that can be fabricated into certain ordered structures, are of great interest, considering their great potential in optics, electronics, biosensors, and thermaology.[1–3] It is well known that conical nanostructures have many outstanding advantages and have been suggested in designs of many instruments, such as thermonuclear fusion control devices, absorbers in solar cells, cold cathodes in field emission displays, and some quantized electrical devices.[4–7] Such applications, however, require materials possessing excellent properties with multiple functions. Conical nanostructured diamond has many outstanding advantages and can be used to construct nanodevices with high functionality for many fields. Diamond has the highest hardness, the highest thermal conductivity, outstanding chemical inertness, wide band gap semiconduction (~ 5.5 eV), and negative electron affinity (NEA). So the interest in diamond nanocones with a high aspect ratio for the above-mentioned application areas is unsurprising, particularly for electrical devices. In this work, the relationships between the cone morphologies and experimental parameters, such as the CH_4/H_2 gas ratio, bias current, and gas pressure are investigated.

2. Preparation of diamond nanocone arrays

Generally, diamond cones can be fabricated by growing diamond into holes patterned on silicon or SiO_2 substrates by micro-fabrication techniques including photo-lithography, reactive ion etching (RIE), wet etching, etc.[8,9] However, the controlled fabrication methods and the understanding of the formation mechanisms of nanoscale conical structures are necessary due to the application requirements for nanodevices. Recently, a novel method for fabrication of diamond cone arrays was realized by combination of focused ions beam (FIB) milling technology and diamond filling, and as-formed diamond morphology can be well controlled by the shape of premilled holes on silicon using an FIB system, while the density of cone arrays can be controlled by the patterning density of the array of holes.[10] On the other hand, dry plasma etching technology without pre-patterning for formation of diamond cone arrays has been studied using different plasmas, such as oxygen and hydrogen, in CVD systems,[11,12] which has a particular potential in the formation of large-area cone arrays, and has been verified as an economical technique for diamond, even though no adequate account of the underlying cone formation mechanism has been given so far.

We developed a novel maskless method to fabricate large-area diamond nanocone arrays with an ordered orientation, a controlled density and a uniform cone angle.[13] As-grown diamond films are placed into a hot filament chemical vapor deposition (HFCVD) chamber equipped with a direct cur-

*Project supported by the National Natural Science Foundation of China (Grant Nos. 51272278, 11174362, and 91023041), the National Basic Research Program of China (Grant No. 2009CB930502), and the Knowledge Innovation Program of the Chinese Academy of Sciences (Grant No. KJCX2-EW-W02).

†Corresponding author. E-mail: czgu@iphy.ac.cn
‡Corresponding author. E-mail: jjli@iphy.ac.cn

rent (dc) negatively biased voltage system; CH_4 is added to the etching gas H_2 to improve the plasma etching intensity and efficiency. Figure 1 shows an SEM image of typical diamond cone arrays formed under the following experimental conditions: CH_4/H_2 ratio of 1.5/98.5, gas pressure of 5 Torr (1 Torr = 1.33322×10^2 Pa), substrate temperature of 900 °C, etching duration of 1 h, and a glow discharge current of 100 mA. It can be clearly seen that the as-formed cones show an identical orientation, a uniform cone angle of about 27°, and a height of about 3 μm; the cone density is about 2×10^8 cm^{-2}. Figure 2(a) is the full TEM image of a single cone in low magnification; an apex radius of about 1 nm is obtained as shown in the inset. Figure 2(b) is the sidewall high-resolution transmission electron microscope (HRTEM) image of a single cone; we can find that the diamond cone is coated by a 1-nm to 2-nm amorphous carbon layer and has a polycrystalline diamond core with the main atom lattice spacing of 0.22 nm, related to the diamond (111).[14] No metal or other particle serving as a mask on the cone top is detected from the TEM image.

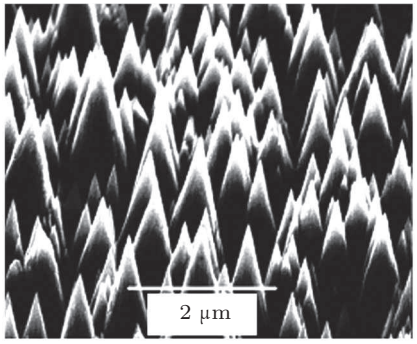

Fig. 1. Typical SEM image of as-formed diamond cone arrays.[13]

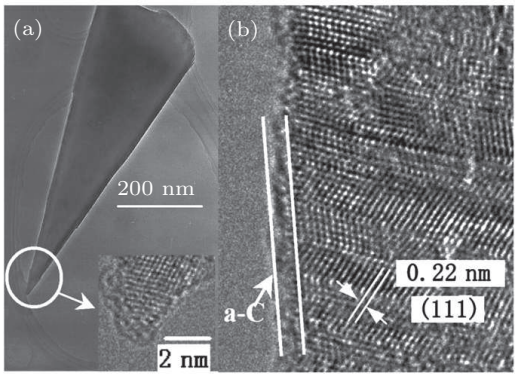

Fig. 2. TEM characterizations of diamond cone: (a) the full image in low magnification inset with an HRTEM image of the cone tip, and (b) HRTEM image of the cone sidewall.[13]

This result indicates that diamond cone arrays with uniform morphology can be formed by using CVD plasma etching, the as-formed cones have a uniform cone angle, height, and distribution. For the formation of diamond cones in HFCVD plasma, a self-organized selective sputtering mechanism has been proposed.[13] During the initiation of cone formation, the surface morphology of as-formed diamond film has played a key role. Hillocks are randomly distributed all over the surface. Under the ion bombardment in the plasma, the removal of material is faster at the side of a hillock than at the top, because the ion-sputtering yield is always higher at an oblique incident angle.[15] As a result, the initial surface morphology is enhanced because of the difference in the sputtering rate. With the advance of further ion sputtering, cone geometry is gradually formed and sharpened. Longer sputtering will cause partial removal of the diamond film, resulting in a reduced cone density. The addition of methane gas (CH_4) in the plasma can greatly enhance the sputter-etching process because the methylic ions have a larger mean free path length, and therefore, higher mean energy for sputtering.[16] The methylic ions will be dominant in the etching of diamond even though their densities are much less than that of H^+ ions in the plasma. Meanwhile, the deposition of amorphous carbon occurs simultaneously with the etching process, and these processes finally form a very thin coating on the outer layer of each diamond cone.

Based on the above studies, we know that the arrays of diamond cones with controlled morphologies, such as the cone angle, the cone height, and the array density, can be obtained, which provides a promising method of nanocone array fabrication for applications in large-area field emitter, gas sensors, quantized nanodevices, etc.

3. Field emission from diamond nanocone arrays

Diamond is an ideal material for electron field emission due to its negative electron affinity, outstanding chemical inertness and maximal thermal conductivity. Electron field emission from diamond has been intensively studied in the last decade.[17,18] However, most of the reported diamond emitters are planar diamond films, irregular ion-etched diamond films or non-uniformly diamond coated silicon tips, all of which reveal inconsistent or poor emission behavior. A good candidate for field emitter arrays should be a structure of high aspect ratio nanostructures in an array of moderate density, because a high aspect ratio pillar and cone structure can introduce local field enhancement effect onto the emitting surface,[19] but a high density of emitters is not beneficial for the improvement of field emission due to the field-screening effect.[20–22] Some researchers have predicated that the field emission will become maximal when the spacing is twice as large as the height of the emitters.[20] However, the field emission properties of arrays of regular high aspect ratio diamond tips arrays and the effect of emitter density on the field-screening have rarely been studied, due to the difficulty of preparing those emitters with different densities.

We measured the field emission of as-formed diamond cone arrays with different densities and compared them with

the performance of unetched diamond films. The current density versus electric field (J–E) and Fowler–Nordheim (FN) plots of all samples are shown in Fig. 3. In Fig. 3(a), it is obvious that as-formed diamond cone arrays formed by CH_4 and H_2 plasma etching have much-enhanced field emission compared with unetched diamond films, because of the high field enhancement factor of sharp diamond cones and the amorphous carbon outer layer in the diamond cones. The cone arrays formed by pure H_2 plasma etching also show enhanced emission, but they have poorer field emission performance than the cones formed by CH_4/H_2 plasma etching, owing to their lower aspect ratio, higher cone density, and lack of outer amorphous carbon coating. The amorphous carbon layer can increase the surface electrical conductivity and provide a pathway for electron-hopping conduction through the defect bands within the wide band gap of local sp^3 sites so as to enhance the field emission ability of the as-formed diamond cones. In general, the FN plots are nearly linear, indicating that electron field emission from these as-formed diamond cone arrays basically follows the FN law. However, some FN plots of as-formed diamond cone arrays are somewhat nonlinear, as shown in Fig. 3(b). This nonlinear FN plot is often observed in some carbon-based materials. Usually, this plot has to be fitted with two straight lines instead of one, each of which can derive its own field enhancement factor (â-value), suggesting that two different types of emission sites are contributing to the total emission current.[16] It can be seen from Fig. 3(a) that the field emission of diamond cones depends on its cone density, diamond cone arrays with higher density (about 2×10^8 cones/cm^2) or lower density (about 2×10^6 cones/cm^2) have higher threshold fields than those of the cone arrays with medium density (about 1×10^7 cones/cm^2). And the emission current densities are also much lower than those of the cone arrays with medium density. The slower current increase of diamond film before etching is similar to cone arrays with density of 2×10^8 cones/cm^2 and the cone arrays formed by pure H_2 plasma etching with cone density larger than 1×10^9 cones/cm^2, and the quicker current increase of cone arrays with density of 2×10^6 cones/cm^2 is similar to that of 1×10^7 cones/cm^2. The above trends are closely related to the field-shielding effect that exists in emitters with a larger emitting site density and to the field enhancement factor determined by the geometrical shape of cones. These phenomena can be attributed mainly to the appropriate balance between the field-shielding effect and the number of field emission sites. High density arrays of cones will lead to a strong field-shielding effect,[20] which reduces the surface field of each individual cone, resulting in low emission current. Low density arrays of cones will have fewer emission sites. Their total emission current is lower, despite a weaker field-shielding effect. There is an optimum cone density at which the maximum emission current can be obtained. In addition, when the cone density of one sample is close to that of another, the field enhancement factor will determine the field emission property of the sample, that is, a higher field enhancement factor leads to better field emission.

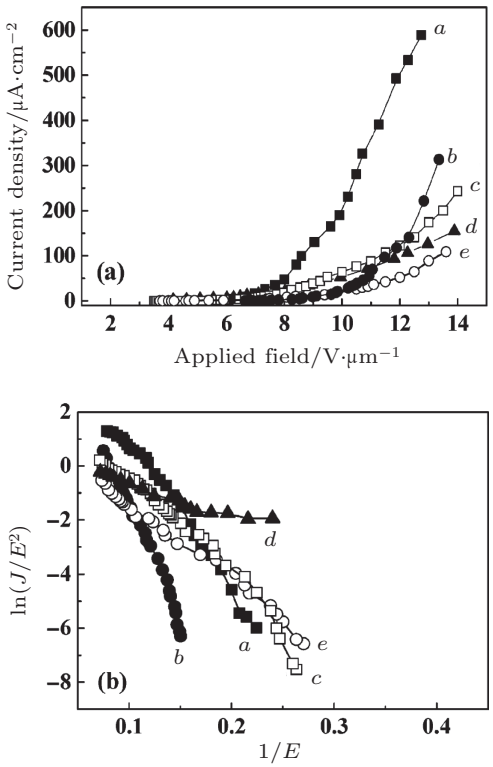

Fig. 3. The J–E characteristics (a) and FN characteristics (b) for the unetched diamond film, diamond film etched in H_2 plasma, and as-formed diamond cone arrays etched in CH_4/H_2 plasma with different cone densities: 1×10^7 cones/cm^2 (curve *a*), 2×10^6 cones/cm^2 (curve *b*), 2×10^8 cones/cm^2 (curve *c*), H plasma etching (curve *d*), diamond film (curve *e*).[16]

4. Field emission from an individual diamond nanocone

Among many applications of vacuum microelectronics, there is a great demand for cold-cathode electron point sources in a variety of scientific instruments. For example, nanoscale probe instruments, which are based on cold-cathode electron point sources, are vital for applications such as ultrahigh resolution electron-beam lithography, electron holography, field electron emission (FEE) microscopy, etc.[23] The key factor for the fabrication of an efficient electron point source is the formation of an atomically sharp field-emission tip. Although remarkable progress has been made in the last few years in the development of high efficiency point emission sources based on either an individual carbon nanotube emitter or a silicon cone emitter coated with materials of negative (or low) electron affinity such as diamond, diamond-like-carbon, etc.[24,25] However, due to the relatively high work function of carbon nanotubes and the low aspect ratio geometry of coated Si emitters, their emission capability is insufficient to work as a single

electron point source. Therefore, the ultimate goal is to make a high-aspect-ratio point-electron-emitter directly from a material with negative electron affinity, such as the diamond.

In our research, the FEE properties of an individual diamond cone have been studied using a customized double probe scanning electron microscope (SEM) system at a chamber pressure of about 10^{-7} Torr. The SEM system is equipped with a microsized anode probe and is more efficient than the conventional anode panel systems in collecting locally emitted electrons.[26] The anode probe has a tip radius of about 1 μm formed by chemical etching of a tungsten wire, and the distance between the anode probe tip and a diamond cone can be adjusted to be as small as 0.1 μm. The emission current was measured by a picoampere meter upon applying a dc voltage between the anode probe and the silicon substrate.

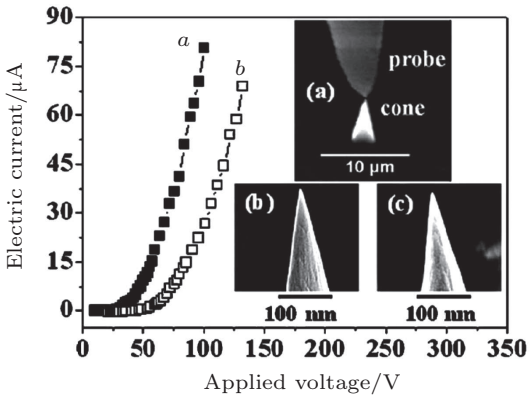

Fig. 4. The *I*–*V* plots of an individual, isolated diamond cone before [plot *a*] and after surface stabilization [plot *b*], with inset SEM images: (a) showing FEE measurement system (anode probe and a diamond cone) and inset high resolution SEM images of the diamond cone before (b) and after (c) FEE measurement.[27]

An as-formed emitter generally needs surface stabilization by means of Joule heating to establish a stable electron emission.[24] Figure 4 shows the *I*–*V* plots of an individual diamond cone before and after the surface stabilization process. The tip-probe measurement setup is shown in the inset (a). Before surface stabilization, the emission current begins to rise quickly at applied voltage of 24 V. At applied voltage of 100 V, a high emission current of about 80 μA is obtained, as shown by the plot *a*. In this experiment, the electrical field at the cone tip is 25 V/μm at the voltage of 10 V between the diamond cone and the anode probe, which is determined using the equation: $\beta E = V/R_{\rm tip}$.[28] The emission current from the individual cone is about 1×10^{-2} μA at 25 V/μm. The field enhancement factor β for a conical structure is expressed: $2.1(h/r+0.8)0.73$,[29] and it is calculated as 325 for the present individual diamond cone, assuming a cone height of 5.1 μm and cone apex radius $R_{\rm tip}$ of 5 nm. At the same electrical field (25 V/μm), Zhang *et al.*[12] reported an emission current density of about 10^2 mA/cm^2 from single-crystal diamond cone arrays, from which the emission current of a single diamond cone can be estimated as 5×10^{-4} μA, assuming a cone density of 2×10^8 cm^{-2}. This indicates that the emission properties of an isolated individual diamond cone are superior due to the exclusion of the field-shielding effect. When the emission is measured several times, its emission ability is degraded a little but very stable, (see plot *b* in Fig. 4). The high emission ability of an as-formed diamond cone can be attributed to the high-aspect-ratio conical structure which introduces an enhanced field at the cone tip; and the *a*–C coating layer which provides pathways for electron hopping conduction through the defect bands within the wide band gap of local sp^3 sites in the cascaded sp^2–sp^3–sp^2 (metal–insulator–metal) surface nanostructure.[30] The results show good promise for these diamond cones to be used as individual point electron sources.

5. Gas sensing properties of diamond nanocone arrays

The notable performance of diamond based sensors in the detection of reducing gases (NH_3, CO, H_2, etc.) and oxidizing gases (O_2, NO_2, HCL, etc.) have been achieved.[31,32] However, limited sensitivity has severely blocked their further development. It has been suggested that the enlargement of the effective sensing area might solve this problem.[33] Nanostructured diamond materials, such as diamond films with conical protrusions, will satisfy this requirement well, due to their greatly enhanced surface aspect ratio.

We studied the gas sensing properties of diamond nanocone arrays. First, the hydrogenation of diamond film and as-formed diamond nanocone arrays in H_2 ambience is performed at the temperature of 800 °C for 0.5 h. Before the measurement of the gas sensing performance, NO_2 and NH_3 gases with a volume of 1 mL were injected separately into a Teflon container (10000 mL), and thus 100 ppm (part per million) air-diluted NO_2 and NH_3 gases were prepared.

The air-ambience current versus voltage (*I*–*V*) characteristics of the diamond film and diamond nanocone arrays (with and without hydrogenation) are illustrated in Fig. 5(a). After hydrogenation in H_2 ambience, the surface conductivity of as-formed diamond nanocone arrays and diamond film is increased by about 3–4 orders, which indicates the formation of a surface conductive layer. For both diamond film and nanocone arrays, rectifying *I*–*V* properties are detected, indicating that Schottky barriers are formed in the metal–semiconductor (diamond-gold wire) contacts. The current versus measurement time (*I*–*t*) plots of diamond film and diamond nanocone arrays, both in air-diluted NH_3 and NO_2 ambience, are shown in Figs. 5(b) and 5(c). From Fig. 5(b), one can see that the current is decreased by 6.1 times for diamond nanocone arrays in NH_3 ambience and it is decreased by 2.9 times for the diamond film. We can also see that for the diamond nanocone arrays the current is increased by about 4.9

times in NO_2 ambience; for diamond film the current is increased by about 3.1 times, as shown in Fig. 5(c).

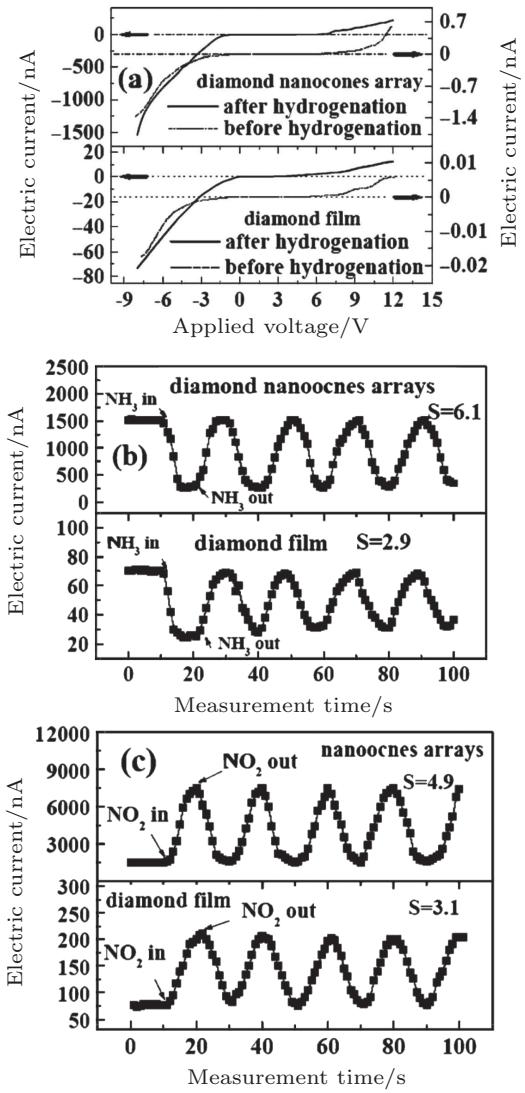

Fig. 5. Sensing properties of a hydrogenated diamond film and a nanocone array at room temperature, *I*–*V* characteristics in air before and after hydrogenation (a), NH_3 sensing *I*–*t* plot (b), and NO_2 sensing *I*–*t* plot (c).[34]

As to the sensing mechanism of the diamond gaseous sensor, it was recently proposed that a surface hydrogenation layer with greatly increased p-type conductivity can play a key role.[35] It has been proposed that hydrogenation could raise the valence band maximum of diamond sufficiently to a place just above the chemical potential of a mildly acidic water layer physisorbed at the surface, and thus produces p-type conductivity.[36] Due to the surface band bending and the formation of an ultrathin (about 5 nm) conducting layer on an insulating diamond substrate, a two-dimensional (2D) hole gas with discrete subbands that will be presented even at room temperature.[37] In the case of diamond nanocones, the further size confinement (cone tip size is about 2 nm as shown in SEM characterization) of the original 2D hole gas due to the formation of a conical structure will introduce further separated hole quantum well states. Carrier transformation between the adsorbed gas and the discrete hole states may be facilitated due to the lower transformation barrier for different subbands. When the p-type diamond surface contacts NH_3 gas, the electrons are transferred from the adsorbed aqueous NH_3 into the diamond nanocone to equalize the chemical potentials (or Fermi levels).[38] Then, the hole concentration is reduced, and consequently, the conductivity of the diamond is reduced. Whereas, when the diamond contacts NO_2 gas, electrons are transferred from the diamond surface into the adsorbed aqueous NO_2, and the conductivity of the diamond is increased accordingly.

6. Quantized tunnel current of diamond nanocones

The nanocontact between a metal and a semiconductor, which has attracted attention not only in terms of its scientific importance but also its applications in quantum device architectures, has been investigated in various systems. Some previous studies have investigated quantum confinement effects via the metal contacts on a homogenous semiconductor substrate and a semiconducting nanostructure such as a quantum well and two-dimensional electron gas (2DEG), both in experiment and in theory.[39,40] However, research on nanocontact systems between metals and wide-band gap semiconductors with high functionality is still in its infancy. The difficulty of fabricating reliable metal-semiconductor nanocontacts has thus far limited the experimental study of such nanocontacts.

In our work, the electron transport properties of a nanocontact between a metal W probe and an individual diamond nanocone have been measured. SEM images of the nanocontact measurements aare shown in Fig. 6. A three-dimensional (3D) moveable W probe can contact different positions of an individual diamond nanocone, from top to bottom.

The I–V_a curves at room temperature (293 K) for different contact configurations between the W probe and the diamond nanocone are plotted in Fig. 7(a). Figures 7(a1)–7(a2) correspond to the contacts of the W probe with the nanocone at the top and midway. The measurement of the diamond film is also presented as a reference, the blue line shown in Fig. 7(a3), corresponding to the contact of the W probe with the diamond film, is the fitted curve based on a tunneling mechanism as suggested in the following discussion. Typical rectifying behavior was found in all three measurements, with forward and reverse bias. For the contact of the W probe with nanocone top [Fig. 7(a1)], current jumps occur at a forward bias of 7.6 V, 19.3 V, and 40.6 V. Comparatively, for the contact between the W probe and the diamond nanocone midway [Fig. 7(a2)], such jumps cannot be clearly identified, as was the case of the contact between the W probe and the diamond film surface [Fig. 7(a3)].

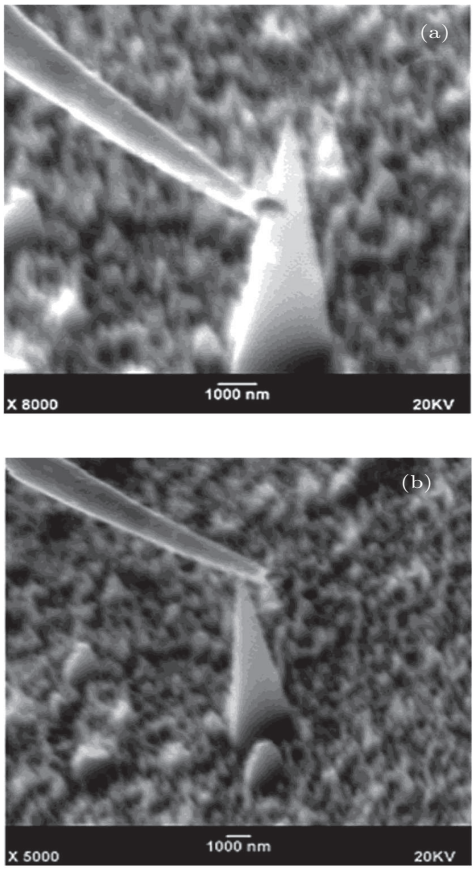

Fig. 6. SEM images of contact configurations of the W probe at the middle (a) and tip (b) of an individual diamond nanocone.

The I–V_a curve of the nanocontact between the W probe and the diamond nanocone tip can be understood as the combination of a smooth background current and some discrete current jumps. The smooth background of the I–V_a curve at forward bias combined with the curve at reversed bias provides us the information about the tunneling barrier.

The temperature dependence of these discrete current jumps was also investigated by changing the substrate temperature. The I–V_a characteristics of the diamond nanocone tip at elevated temperature are shown in Fig. 7(b), the dashed lines shown in Fig. 7(b) are the curves numerically fitted by using the tunneling current at 293 K from different discrete hole levels as suggested in the flowing discussion. From Fig. 7(b), the following results can be obtained: (i) the background current is enhanced at the elevated temperatures of 393 K and 493 K; (ii) the current jumps observed at 293 K disappear at elevated temperatures of 393 K and 493 K.

Here, a tunneling process from discrete hole levels in the diamond nanocone tip to the W probe is suggested to explain the as-observed experimental results. The contact between the hydrogenated diamond nanocone tip and the W probe can be though of as a quantum point contact (QPC) structure as illustrated in Fig. 8(a). The hydrogenated diamond tip can be considered as a quantum dot. The nanocone body beneath the tip, which is formed by stacking diamond crystallites with many defects,[28] acts as the other electrode for this QPC structure. Discrete electron states will be formed due to the size confinement within the diamond nanocone tip. The existence of the p-type region is due to the electrochemical transfer doping effect,[41] which results in upward band bending at the interface of the diamond nanocone and the W probe. It should be noted that the W probe could be easily covered with an oxidized layer several nanometers thick due to air exposure.[42] That would act as an insulating barrier, which indicates a metal–insulator–semiconductor (MIS) nanostructure formed at the contact between the diamond nanocone and the W probe as shown in Fig. 8(b).

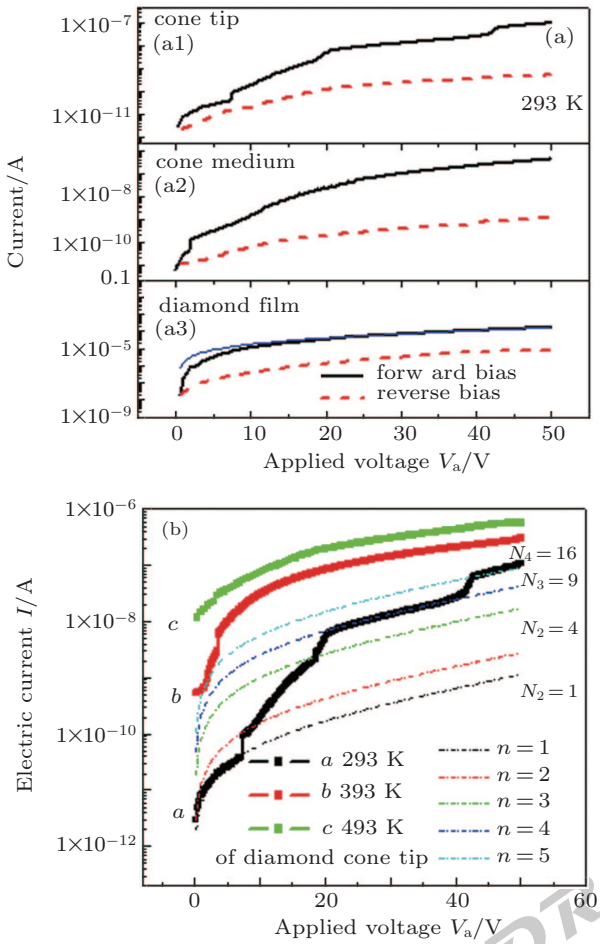

Fig. 7. (a) The I–V_a plots of different contact configurations at forward (solid lines) and reverse (broken lines) biases at room temperature: (a1) the contact of the W probe with the diamond nanocone tip, (a2) the contact of the W probe with the diamond nanocone midway, and (a3) the contact of the W probe with diamond film. (Blue line is a fitted curve based on the tunneling model.) (b) The I–V_a plots of the contact of the W probe with the diamond nanocone tip at different temperatures: 293 K (curve *a*, dashed lines are the fitted I–V_a plots based on the tunneling model); 393 K (curve *b*), and 493 K (curve *c*).

At zero bias, most discrete hole energy levels at the diamond nanocone side are above the Fermi level, and they cannot participate in the tunneling process. Due to the increase of the applied forward bias on the diamond nanocone, the Fermi level at the metal side is elevated. As a result, more

and more quantized hole levels take part in the tunneling process, as in the schematic in Fig. 8(c). This produces the current jumps as observed, appended on the smooth background current through a trapezoid surface barrier, as shown in Fig. 7(a1).

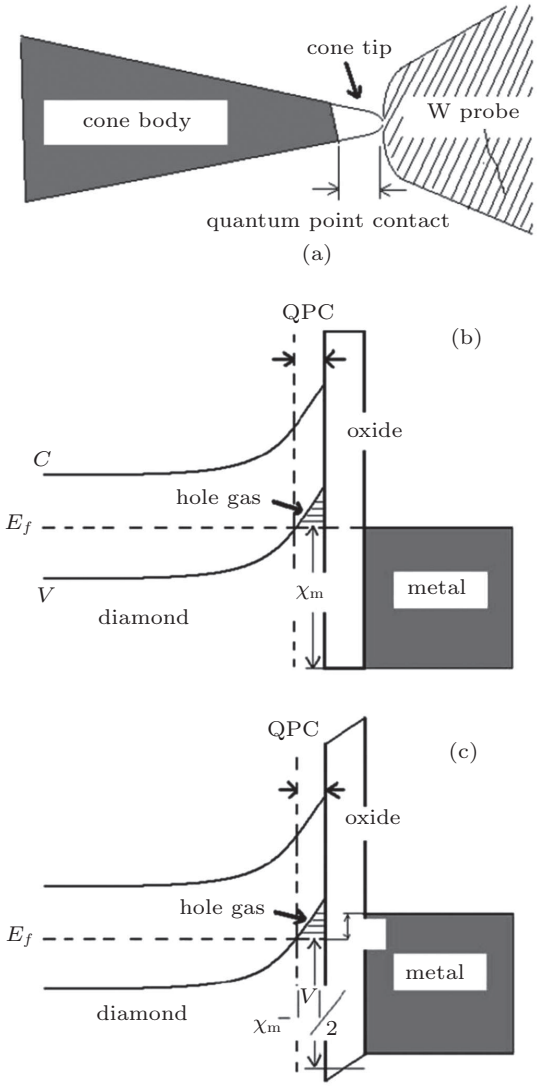

Fig. 8. Schematic diagram of nanocontact structure (a) and energy-band diagrams of the nanocontact with an insulating barrier between the diamond cone tip and the W probe at zero bias (b) and negative (c) bias.

Assuming a QPC structure, spatial confinement will lead to the quantization of original hole gas. The discrete energy levels in a quantum dot can be expressed as[43]

$$E_n \propto \frac{h^2 n^2}{8m^* r^2} \quad (n = 1, 2, 3, \ldots). \tag{1}$$

Here, m^*, the hole effective mass perpendicular to the surface, is 0.75 m_e,[38,44] r is the tip radius of the diamond cone, and h is the Planck's constant. The averaged tip radius measured from SEM images yields $r \approx 2.5$ nm. The degeneracy of the discrete states is $N_n = n^2$.

As has been well known, with the increase in the measurement temperature, thermally excited carriers can disturb the original discrete hole carriers states Planck's constant, concealing the quantized carrier transport process. Therefore, it is rather difficult to preserve a well-defined quantum structure at room temperature. However, in our case, under the assumption of the QPC with a cone tip radius of 2.5 nm, the energy gap of the first two levels is estimated to be about 0.114 eV (much larger than the thermal disturbance of about 0.026 eV at room temperature), so the as-formed quantum states in the diamond tip QPC structure can be preserved well even at room temperature due to the rather small confined dimension. Applying an external electric field is an effective way to extract hole carriers from the as-formed QW states through the surface tunneling process. The applied (negative) bias on the W probe can modulate the position of the Fermi level in the above-mentioned QPC system and cause new hole energy states in the QPC structure to contribute to the total tunneling current, as schematically shown in Fig. 8(c).

The electron transport through the nanocontact is a rather complicated problem. It is very difficult to find out how the localized QW states couple to the states of the diamond cone surface through defects of the cone. However, a simple but very useful formulism was developed in field emission research on diamond. Similar to the description in Refs. [45] and [46], the tunneling current can be expressed as

$$J(V) = A \sum_{i=1}^{m} N_i T_t(E_i, V) f(E_i, V), \tag{2}$$

where A is the contact area and $N_i = i^2$ is the number of states at E_i, $f(E_i, V)$ is the attempted escape frequency of this energy level, stemming from the classical expression of the oscillation frequency of localized states. It can be calculated as[38]

$$f(E_i, V) = \frac{eV}{2d\sqrt{2m_h^* E_i}}, \tag{3}$$

with d being the barrier width, assumed to be 1.5 nm, and $T_t(E_i, V)$ the tunneling coefficient of the trapezoid barrier from the i-th subband. In Wentzel–Kramers–Brillouin (WKB) approximation, the tunneling transmission coefficient T_t of the trapezoid barrier (with barrier height of $\psi_1 = \chi_m + E_i + kT$ and $\psi_2 = \chi_m + E_i + kT + e|V|$) is a function of the applied field V[47]

$$T_t(E_i, V) \approx \exp\left[-\sqrt{2}\left(\frac{8\pi^2 m_h^*}{h^2}\right)^{1/2} (\Psi_1 + \Psi_2)^{1/2} d\right]. \tag{4}$$

Here, m_h^* is the effective hole mass with value of 0.75 m_e (m_e is the free electron mass),[38] E is the hole energy, and h is Planck constant, $\psi_2 = \chi_m + E_i + kT + e|V|/2$ is the average tunneling barrier height at applied voltage V (χ_m, the barrier height of the Fermi level, and $\chi_m > |V|$), k is the Boltzmann constant, T is the absolute temperature. From the above formulism, it is

inferred that discrete current jumps can be observed at a certain applied voltage gap of $(E_i - E_{i+1})/e$.

Assuming that the voltage applied on the nanocontact is proportional to the total voltage applied to the device, we define $\beta = V/V_a$, where V is the voltage applied on the tunneling contact, and V_a is the total voltage on the two metal electrodes. Then, by a polynomial fitting [by using Eq. (2)] of curve *a* in Fig. 7(b), we find that $\chi_m = 1.54$ eV and $\beta = 0.0106$ can well produce our experiment results shown in Fig. 7(b). In addition, $\chi_m = 1.54$ eV can be used to produce the $I - V_a$ curves of diamond film (with $\beta = 0.3$), as shown in Fig. 7(a3).

The discrete current jumps can be explained quite well by considering discrete hole levels, as shown in the fit lines plotted in Fig. 7(b). The observed current jumps at 7.6 V, 19.3 V, and 40.6 V indicate subband gaps of 0.103 eV and 0.194 eV, indicating an inter-subband gap ratio of about 3:5. This fits $(E_2 - E_1)/(E_3 - E_2)$ well, as calculated from Eq. (1).

Thus, the result at the room temperature shown in Fig. 7(b) can be well explained by employing the above-discussed tunneling mechanism. At elevated temperature, the tunneling barrier is decreased, which increases the tunneling coefficient T_t, as indicated from Eq. (4). Thereafter, the tunneling current at elevated temperature will be enhanced. However, the thermally excited carriers at elevated temperature will conceal the discrete current jumps observed at room temperature. It seems that no dehydrogenation process occurs at the surface of the diamond nanocone at elevated temperature, because no current decrease is observed even at the temperature of 493 K, which accords well with the results reported by Cui *et al.*[48]

7. Conclusions

The electrical properties of ordered diamond cone arrays self-organized under selective ion sputtering, using the HFCVD system, have been reviewed. The following conclusions can be drawn.

(i) Diamond cones with different aspect ratios and cone densities can be formed by HFCVD plasma etching with CH_4/H_2 gas mixture. The addition of CH_4 can effectively enhance plasma etching. The enhancement is attributed mainly to the mean energy of methylic ions being higher than that of H^+ ions. The aspect ratio and density of diamond cones can be controlled by the duration of ion sputtering. Another advantage of adding methane gas to the plasma is the formation of a thin amorphous carbon coating over the diamond cones, which is favorable to the enhancement of field emission by providing a pathway for electron-hopping conduction through the defect bands.

(ii) Compared with the unetched diamond film, as-formed diamond cones have enhanced field electron emission with good emission stability. The diamond cones formed by CH_4/H_2 plasma etching have a better field emission property than those formed by pure H_2 plasma etching because of a more advantageous cone array density and a higher field enhancement factor. The threshold field for electron emission depends on the distribution density of diamond cones because of the field-shielding effect.

(iii) High emission current can be obtained from an individual diamond cone due to its high-aspect-ratio geometry and the electron conducting pathway provided by the *a*–C covering layer with high content of sp^2 bonding. After a surface stabilization process, the diamond cone shows stable emission properties and a stable work function of 3.35 eV, due to both the desorption of surface H atoms and the loss of sp^3 emitting sites.

(iv) The chemical gas sensing properties of as-formed diamond nanocone arrays show that the enhanced gas sensing performance is obtained due both to the carriers tunneling from discrete hole states in the diamond nanocone and to the enhanced surface-to-volume ratio of the conical structure.

(v) The observed current-jumps in the I–V_a plots directly reflect the presence of quantum well states in the nanocontact structure between the diamond nanocone tip and the W probe. The results also indicate that the number of current jumps clearly show the nanocontact size and temperature dependence – that is, with the contact size and measurement temperature increasing, the jumps are more difficult to observe, due to the decreased sub-band gap and thermal disturbance. The results can be theoretically reproduced quite well by using the tunneling mechanism of discrete hole levels in the nanocontact structure.

In summary, the nanostructured diamond cones show great potentials for the application as unique nanodevices.

References

[1] Iijima S 1991 *Nature* **354** 56
[2] Rangelow I W 2001 *J. Vac. Sci. Technol. B* **19** 916
[3] Huq S E, Kent B J, Stevens R, Lawes R A, Xu N S and She J C 2001 *J. Vac. Sci. Technol. B* **19** 988
[4] Wong W K 2002 *Appl. Phys. Lett.* **80** 877
[5] Zhu J 2009 *Nano Lett.* **9** 279
[6] Lu C, Li Y L, Tian S B, Li W X, Li J J and Gu C Z 2011 *Microelectron. Eng.* **88** 2319
[7] Wang Y 2010 *Nano Res.* **3** 520
[8] Sandhu G S and Chu W K 1989 *Appl. Phys. Lett.* **55** 437
[9] Ramesham R and Loo B H 1992 *J. Electrochem. Soc.* **139** 1988
[10] Wang Z L, Gu C Z, Li J J and Cui Z 2005 *Microelectron. Eng.* **78** 353
[11] Baik E S, Baik Y J and Jeon D 1999 *Diamond Relat. Mater.* **8** 2169
[12] Zhang W J, Meng X M, Chan C Y, Wu Y, Bello I and Lee S T 2003 *Appl. Phys. Lett.* **82** 2622
[13] Wang Q, Gu C Z, Xu Z, Li J J, Wang Z L, Bai X D and Cui Z 2006 *J. Appl. Phys.* **100** 034312
[14] Ternyak O, Cimmino A A, Prawer S and Hoffman A 2005 *Diamond Relat. Mater.* **14** 272
[15] Cui Z 2006 *Micro-nanofabrication Technologies and Applications* (Springer-Verlag: Berlin and Heidelberg)
[16] Wang Q, Li J J, Li Y L, Wang Z L, Gu C Z and Cui Z 2007 *J. Phys. Chem. C* **111** 7058
[17] Fox N A, Wang W N, Davis T J, Steeds J W and May P W 1997 *Appl. Phys. Lett.* **71** 2337

[18] Liu N, Ma Z, Chu X, Hu T, Xue Z, Jiang X and Pang S 1994 *J. Vac. Sci. Technol. B* **12** 1712
[19] Geis M W, Efremow N N, Krohn K E, Twichell J C, Lyszczarz T M, Kalish R, Greer J A and Tabai M D 1998 *Nature* **393** 431
[20] Nilsson L, Groening O, Emmenegger C, Kuettel O, Schaller E, Schlapbach L, Kind H, Bonard J M and Kern K 2000 *Appl. Phys. Lett.* **76** 2071
[21] Suh J S, Jeong K S, Lee J S and Han I 2002 *Appl. Phys. Lett.* **80** 2392
[22] Jo S H, Tu Y, Huang Z P, Carnahan D L, Wang D Z and Ren Z F 2003 *Appl. Phys. Lett.* **82** 3520
[23] Nisson L, Groening O, Emmenegger C, Kuettel O, Schaller E, Schlapbach L, Kind H, Bonard J M and Kern K S 2000 *Appl. Phys. Lett.* **76** 2071
[24] Pan L H, Peridier V J and Sullivan T E 2005 *Phys. Rev. B* **49** 57
[25] Semet V, Binh V T, Vincent P, Guillot D, Teo K B K, Chhowalla M, Amaratunga G A J, Milne W I, Legagneux P and Pribat D 2002 *Appl. Phys. Lett.* **81** 343
[26] Karabutov A V, Frolov V D, Simakin A V and Shafeev G A 2003 *J. Vac. Sci. Technol. B* **21** 449
[27] Li H, Li J J and Gu C Z 2005 *Carbon* **43** 849
[28] Wang Q, Wang Z L, Li J J, Huang Y, Li Y L, Gu C Z and Cui Z 2006 *Appl. Phys. Lett.* **89** 063105
[29] Hsieh C T and Chen J M 2003 *Appl. Phys. Lett.* **83** 3383
[30] Edgcombe C J and Valdré U 2002 *Philos. Mag. B* **82** 987
[31] Wisitsora A, Kang W P, Davidson J L and Kerns D V 1997 *Appl. Phys. Lett.* **71** 3394
[32] Gi R S, Ishikawa T, Tanaka S, Kimura T, Akiba Y and Iida M 1997 *Jpn. J. Appl. Phys.* **36** 2057
[33] Song K S, Sakai T, Kanazawa H, Araki Y, Umezawa H, Tachiki M and Kawarada H 2003 *Biosens. Bioelectron.* **19** 137
[34] Metzger L, Fischer F and Mokwa W 2007 *Sens. Actuators A* **133** 259
[35] Wang Q, Qu S L, Fu S Y, Liu W J, Li J J and Gu C Z 2007 *J. Appl. Phys.* **102** 103714
[36] Denisenko A, Aleksov A and Kohn E 2001 *Diamond Relat. Mater.* **10** 667
[37] Maier F, Riedel M, Mantel B, Ristein J and Ley L 2000 *Phys. Rev. Lett.* **85** 3472
[38] Gan L, Baskin E, Saguy C and Kalish R 2006 *Phys. Rev. Lett.* **96** 196808
[39] van Weeks B J, Kouwenhoven L P, Houten H V, Beenakker C W, Mooij J E, Foxon C T and Harris J J 1998 *Phys. Rev. B* **38** 3625
[40] Tivarus C, Pelz J P, Hudait M K and Ringel S A 2005 *Phys. Rev. Lett.* **94** 206803
[41] Maier F, Ristein J and Ley L 2001 *Phys. Rev. B* **64** 165411
[42] Dagata J and Tseng W 1993 *Appl. Phys. Lett.* **62** 591
[43] Ferry D K and Goodnick S M 1997 *Transport in Nanostructures* (Cambridge: Cambridge University Press)
[44] Collins A T 1994 *Properties and Growth of Diamond* (London: INSPEC)
[45] Svistunov V M, Khachaturov A I and Chemyak O I 1998 *Low Temperature Phys.* **24** 501
[46] Litovchenko V G and Kryuchenko Y V 1993 *J. Vac. Sci. Technol. B* **11** 362
[47] Kumar V and Dahlke W 1977 *Solid State Electron.* **20** 143
[48] Cui J, Ristein J and Ley L 1999 *Phys. Rev. B* **60** 16135

Chinese Physics B

Volume 22 Number 9 September 2013

(*Continued on the Bookbinding Inside Back Cover*)

(*Continued on the Bookbinding Inside Back Cover*)

(*Continued on the Bookbinding Inside Back Cover*)

(*Continued on the Bookbinding Inside Back Cover*)

(*Continued on the Bookbinding Inside Back Cover*)

(*Continued on the Bookbinding Inside Back Cover*)

(*Continued on the Bookbinding Inside Back Cover*)

GEOPHYSICS, ASTRONOMY, AND ASTROPHYSICS